

Partial dissociation of water on $\text{Fe}_3\text{O}_4(001)$: adsorbate induced charge and orbital order

Narasimham Mulakaluri,^{1,2} Rossitza Pentcheva,^{1,*} Maria Wieland,¹ Wolfgang Moritz,¹ and Matthias Scheffler²

¹*Dept. of Earth and Environmental Sciences, University of Munich, Theresienstr. 41, 80333 Munich, Germany*

²*Fritz-Haber-Institut der Max-Planck-Gesellschaft, Faradayweg 4-6, D-14195 Berlin, Germany*

(Dated: November 8, 2018)

The interaction of water with $\text{Fe}_3\text{O}_4(001)$ is studied by density functional theory (DFT) calculations including an on-site Coulomb term. For isolated molecules dissociative adsorption is strongly promoted at surface defect sites, while at higher coverages a hydrogen-bonded network forms with alternating molecular and dissociated species. This mixed adsorption mode and a suppression of the $(\sqrt{2} \times \sqrt{2})R45^\circ$ -reconstruction are confirmed by a quantitative low energy electron diffraction (LEED) analysis. Adsorbate induced electron transfer processes add a new dimension towards understanding the catalytic activity of magnetite(001).

PACS numbers: 68.43.Bc, 68.47.Gh, 73.20.-r, 68.35.Md, 61.05.jh

Magnetite has attracted continued interest in the past decades due to its fascinating properties: The high temperature phase is predicted to be a half-metallic ferrimagnet [1] with high magnetic ordering temperature. At around 120 K it undergoes the so called Verwey transition [2]. Both the type of transition (metal-to-insulator vs. semiconductor-to-semiconductor [3, 4]) and the type of charge (CO) and orbital ordering (OO) at the octahedral iron sites in the low temperature phase are subject of an ongoing debate [5, 6, 7, 8].

Besides its applications in magnetic recording and as a prospective material for spintronics, magnetite acts as a catalyst e.g. in environmental redox reactions [9, 10], or in the water gas phase shift reaction [11]. Typically these reactions take place in an aqueous environment prompting the need to understand how water interacts with the Fe_3O_4 -surface. Water can bind to a surface in different modes (e.g. molecular or dissociative) leading to a variety of functional groups that can affect significantly the surface properties and availability of reaction sites and result in a complex surface chemistry [12, 13].

The catalytic activity of magnetite is typically related to the presence of both ferrous and ferric iron in its inverse spinel structure. In the [001]-direction two types of layers alternate: A-layers with tetrahedral iron (Fe_A^{3+}) and B-layers containing oxygen and octahedral iron ($\text{Fe}_B^{2+,3+}$). Both bulk truncations of $\text{Fe}_3\text{O}_4(001)$, either with an A- or a B-layer are polar of type three according to the classification of Tasker [14]. To explain the origin of the $(\sqrt{2} \times \sqrt{2})R45^\circ$ -reconstruction previous surface models proposed an ordering of surface defects (e.g. [15, 16]). Recently, DFT calculations [17, 18] have shown that the symmetry lowering at $\text{Fe}_3\text{O}_4(001)$ is achieved rather by a distorted B-layer, supported also by surface x-ray diffraction [17], LEED [19] and scanning tunneling microscopy (STM) [20].

Despite its importance, only a few studies have addressed the interaction of water with $\text{Fe}_3\text{O}_4(001)$. While initial adsorption was related to surface defect sites, an extensive hydroxylation was reported from x-ray photoemission experiments (XPS) beyond a threshold pressure of $10^{-3} - 10^{-4}$ mbar[21]. Both this study and temperature programmed desorption (TPD) measurements[22] indicate multiple adsorbate sites on the surface. Molecular dynamics simulations with empirical potentials [23, 24] point towards a dissociative adsorption. However, such studies cannot provide reliable information on the energetics and underlying electronic phenomena.

Here we address these fundamental questions within a combined DFT and LEED approach. By varying the coverage and adsorbate configuration of water molecules we compile a surface phase diagram in the framework of *ab initio* thermodynamics. The results show that isolated molecules dissociate on the clean $\text{Fe}_3\text{O}_4(001)$ surface. This process is strongly favored at oxygen vacancies. With increasing coverage a crossover to a mixed adsorption (both molecular and dissociative) takes place that is confirmed in a quantitative LEED analysis. LEED shows also a strong suppression of the $(\sqrt{2} \times \sqrt{2})R45^\circ$ surface reconstruction. Furthermore we find that the adsorbed species invoke electron transfer processes in the subsurface layers resulting in an unique charge and orbital order that may have important implications on the catalytic activity of the surface.

DFT calculations were performed using the full potential linear augmented plane wave method in the WIEN2K [25] implementation. The generalised gradient approximation (GGA-PBE) [26] of the exchange-correlation potential is used. Systematic studies [27, 28] show that the PBE functional gives a good description of hydrogen bonding w.r.t. equilibrium geometries. The error of overbinding which can be as large as 20 meV/bond will not affect our conclusions. Because magnetite is a strongly correlated material we have explored the influence of electronic correlations within LDA/GGA+*U* [29] using $U = 5$ eV and $J = 1$ eV [30], similar to values used

*Electronic address: pentcheva@lrz.uni-muenchen.de

for bulk Fe_3O_4 [6, 7, 31]. The surfaces were modelled in the supercell geometry with slabs containing seven B-layers and six A-layers separated by a vacuum region of 10-12 Å [32]. The positions of adsorbates and the atoms in the outer two BA-layers were relaxed.

We have compared the stability of more than 30 different configurations using *ab initio* thermodynamics [33]. The surface energy, $\gamma(T, p) = \frac{1}{2A} \left(G_{\text{Fe}_3\text{O}_4(001)}^{\text{slab}} - N_{\text{Fe}}\mu_{\text{Fe}} - N_{\text{O}}\mu_{\text{O}} - N_{\text{H}_2\text{O}}\mu_{\text{H}_2\text{O}} \right)$ depends on the Gibbs free energy and the chemical potentials of the constituents. The Gibbs free energy can be expressed through the total energy from the DFT-calculations [33]. Because there are two species in the gas phase, O_2 and H_2O , the surface phase diagram is three dimensional. Fig. 1 displays a two dimensional projection with the most stable configurations for given μ_{O} , $\mu_{\text{H}_2\text{O}}$. We first consider the termination of the clean surface as a function of oxygen pressure. As discussed previously, a modified B-layer (denoted as B) showing lateral and vertical distortions in the surface layer with a *wave-like* pattern is favored over a broad range of oxygen pressures. However, at oxygen poor conditions a B-layer with oxygen vacancies ($\text{B}+\text{V}_{\text{O}}$) is stabilized. This defective surface, previously proposed in a STM study [16], shows dramatic relaxations where the oxygen opposite the vacancy moves towards the Fe_{B} -row by ~ 0.8 Å. Starting from these two terminations [34], we have adsorbed water molecules, varying their concentration and geometry. We find a strong tendency for isolated molecules to dissociate in surface oxygen vacancies ($\text{V}_{\text{O}}+\text{OH}$) whereby a proton diffuses to a surface oxygen (O^{S}) further away and forms a surface OH-group ($\text{O}^{\text{S}}+\text{H}$). Thus, even at very low water vapor pressures, all surface defects are expected to be filled with OH-groups, consistent with XPS results [21]. The dissociation of water in the defect sites invokes significant changes in the electronic structure as shown in Fig. 2a and c, involving the 1π and 3σ molecular orbitals of the OH groups and a switching from Fe^{3+} to Fe^{2+} of $\text{Fe}_{\text{B}}\text{S}-1$ underneath $\text{O}^{\text{S}}+\text{H}$.

The adsorbate-adsorbate interaction that sets in, when a second molecule is adsorbed within the $(\sqrt{2} \times \sqrt{2})R45^\circ$ unit cell, leads to a mixed adsorption mode: One molecule dissociates protonating a surface oxygen, while the intact molecule forms a hydrogen bond with the OH-group. The main part of the phase diagram is dominated by a mixed adsorption mode of four water molecules where all surface Fe_{B} -sites ($\text{Fe}_{\text{B}}\text{S}$) are saturated ($\text{B}+4\text{H}_2\text{O}(\text{M})$). Full dissociation is 12 meV/Å² less stable. Full hydroxylation of the surface is also not likely to occur as the formation of a surface OH-group neighboring a subsurface Fe_{A} is extremely unfavorable.

The electron density redistribution with respect to the B-layer in Fig. 2b indicates a weak charge accumulation between $\text{Fe}_{\text{B}}\text{S}$ and the water molecule (O^{w}), but the strongest charge rearrangement takes place between Fe_{B} and the OH-group (O^{OH}) of the dissociated molecule, in-

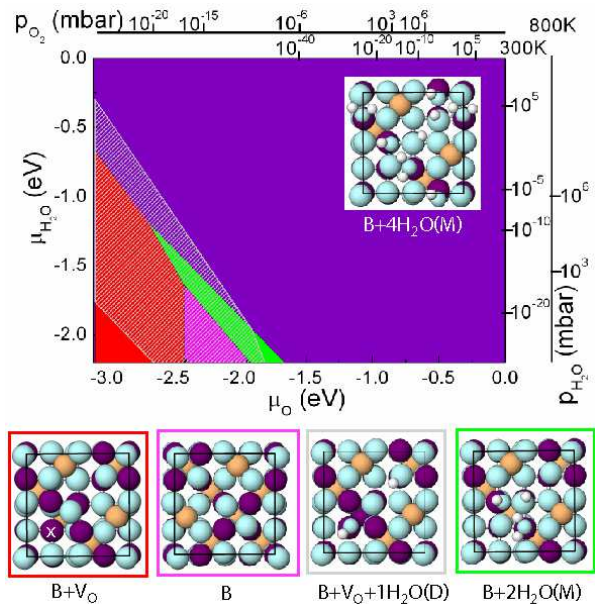


FIG. 1: Bottom view of the surface phase diagram of $\text{Fe}_3\text{O}_4(001)$ showing the most stable configurations for given $(\mu_{\text{O}}, \mu_{\text{H}_2\text{O}})$: $\text{B}+\text{V}_{\text{O}}$ (red), B-layer (magenta), dissociated molecule in an oxygen vacancy $\text{B}+\text{V}_{\text{O}} + 1\text{H}_2\text{O}(\text{D})$ (grey hatched semitransparent area), mixed adsorption of two (green) and four water molecules on a B-layer (purple). The ranges of μ_{O} and $\mu_{\text{H}_2\text{O}}$ correspond to the vapor phase of H_2O . μ_{O} and $\mu_{\text{H}_2\text{O}}$ have been converted into pressures for 300 and 800 K. Additionally, the top views of the most stable configurations are displayed with positions of O, Fe_{B} , Fe_{A} and H marked by cyan, purple, orange and white circles, respectively. In $\text{B}+\text{V}_{\text{O}}$ a white cross marks the position of the vacancy.

volving depletion of 3σ and accumulation in 1π molecular orbitals of OH along with depletion of the d_{z^2} orbital at $\text{Fe}_{\text{B}}\text{S}$. The main actuator of partial dissociation appears to be the formation of strong intermolecular hydrogen bonds. As a result both H_2O and OH tilt from the on-top position towards each other and $\text{O}^{\text{w}}-\text{H}$ elongates from 0.95 Å (gas phase) to 1.10 Å, resulting in an $\text{O}^{\text{w}}-\text{H}\cdots\text{O}^{\text{OH}}$ of 2.47 Å. A fingerprint of the mixed adsorption are the two distinct bond lengths between $\text{Fe}_{\text{B}}-\text{O}^{\text{w}}$ and $\text{Fe}_{\text{B}}-\text{O}^{\text{OH}}$ of 2.09 Å and 1.97 Å respectively. This feature is confirmed by the LEED analysis described below.

LEED measurements were performed on a synthetic magnetite sample. The clean surface, prepared by Ar^+ -ion sputtering and subsequent annealing at 900-1000 K at $p_{\text{O}_2} = 5 \times 10^{-7}$ mbar for 2-3 h, exhibited a $(\sqrt{2} \times \sqrt{2})R45^\circ$ -LEED pattern with sharp superstructure reflections and low background (Fig. 3 a). Water was adsorbed at 273 K for 2 min at a water vapor pressure of 2×10^{-6} mbar, resulting in a (1×1) -LEED pattern with an enhanced background (Fig. 3b). While annealing up to 770 K restores the superstructure spots, the shape of the the LEED $I(V)$ curves cannot be recovered [37], indicating some residual hydroxylation of the

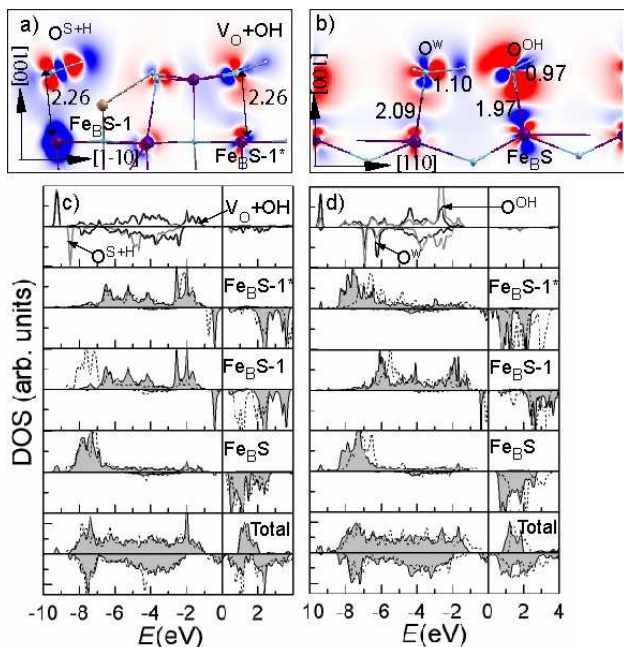


FIG. 2: Adsorbate induced electron density redistribution for (a) B+V_O+1H₂O(D) and (b) B+4H₂O(M). Red/blue corresponds to regions of charge accumulation/depletion. Relevant bond lengths are given in Å. Total and projected density of states (DOS) before (dashed line) and after water adsorption (solid line, grey area) for (c) B+V_O+1H₂O(D) and (d) B+4H₂O(M). S (S-1) denote surface (subsurface) Fe_B sites.

surface, as observed by Kendelewicz *et al.* [21]. Seven LEED $I(V)$ curves of the (1×1) -surface were measured in the energy range 50 - 300 eV at 100 K. An increase of the background current during the measurement is attributed to uncorrelated defects induced by the electron beam [38]. However, no changes were observed in the LEED $I(V)$ curves during repeated measurements over periods of several hours.

LEED calculations were performed with the layer doubling method and a least squares optimization [35] using constraints for bond lengths. The crystal potential was calculated from a superposition of atomic potentials using optimized muffin-tin radii [36] which led to reliable structural determination of the clean Fe₃O₄(001)-surface [19]. 10 phase shifts were used. All positions and occupation numbers within the adsorbate and top B-A-B substrate layers were optimized in a $(\sqrt{2} \times \sqrt{2})R45^\circ$ -unit cell, while thermal parameters were kept fixed. The best fit ($R_P = 0.27$) was obtained for a model where all Fe_BS sites have adsorbed oxygen on top. Both the surface Fe_B- and adsorbate sites are occupied by $\sim 80\%$ possibly due to defect creation during the preparation procedure. The adsorbed O shows strong lateral shifts by ~ 0.4 Å off the Fe_B sites in agreement with the DFT results (0.23-0.28 Å). The main feature are the two different bond lengths Fe_B-O^w/O^{OH}: 2.12 Å and 1.93 Å, confirming the simultaneous occurrence of hydroxyl groups and molecular adsorption. Further details on the structural analysis

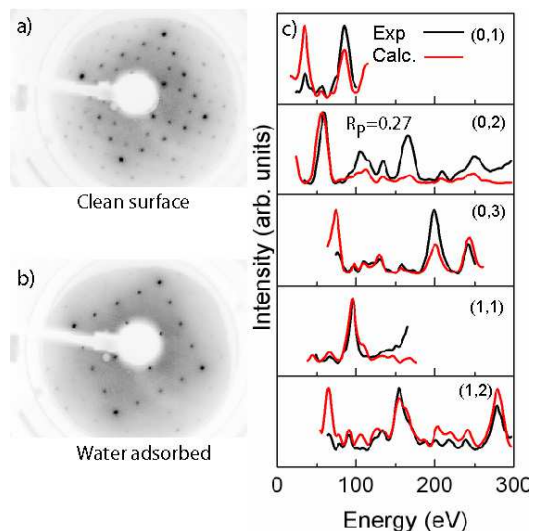


FIG. 3: (Color online) LEED pattern a) before and b) after water adsorption. The superstructure spots in a) indicative of the $(\sqrt{2} \times \sqrt{2})R45^\circ$ surface reconstruction are largely suppressed in b). c) experimental (averaged over symmetrically equivalent beams - black) and calculated (red/grey) LEED $I(V)$ curves of the water adsorbed surface.

will be published elsewhere [37].

We turn next to the surface and adsorbate induced electronic effects on Fe₃O₄(001). The electron density plot in Fig. 4 displays the minority t_{2g} occupancies at the Fe_B-sites, thus allowing to distinguish between sites with predominant Fe²⁺ or Fe³⁺-character [30]. The notation Fe²⁺ and Fe³⁺ is used here for simplicity, but the difference in total 3d occupation within the muffin-tin sphere is much smaller (0.2-0.4e) consistent with XRD- [5] and LDA+*U* studies for the low temperature bulk phase [6, 7]. The magnetic moments allow a clearer discrimination: $M_{\text{Fe}^{2+}} = 3.54 - 3.75\mu_B$, $M_{\text{Fe}^{3+}} = 3.90 - 4.10\mu_B$, respectively. For most of the stable systems we find that the surface layer contains exclusively Fe³⁺ while a unique charge and orbitally ordered state emerges in the deeper layers depending on the type of termination [39]. In B+V_O (Fig. 4a) the two subsurface Fe_B next to V_O are Fe²⁺ ($d_{xz} \pm d_{yz}$). Upon water adsorption the positions of Fe²⁺ switch in B+V_O+1H₂O(D): now the two Fe_B below the surface OH groups are Fe²⁺, resulting in alternating Fe²⁺, Fe³⁺-sites. In the mixed adsorption case (B+4H₂O(M)) the charge ordering in the subsurface layer is not significantly altered compared to B-layer, where one out of four Fe_BS-1 is Fe²⁺ and a second is in an intermediate valence state. However, the slight tilting of the t_{2g} orbital at Fe_B²⁺ induces a completely different OO in S-2: from $d_{xz} \pm d_{yz}$ to alternating d_{xy} and d_{xz} -orbitals. Recent GGA+*U* calculations have shown that in bulk magnetite a variety of CO/OO states can be realized by symmetry lowering [31]. Here the presence of a surface and adsorbates imposes a unique CO/OO state for each ter-

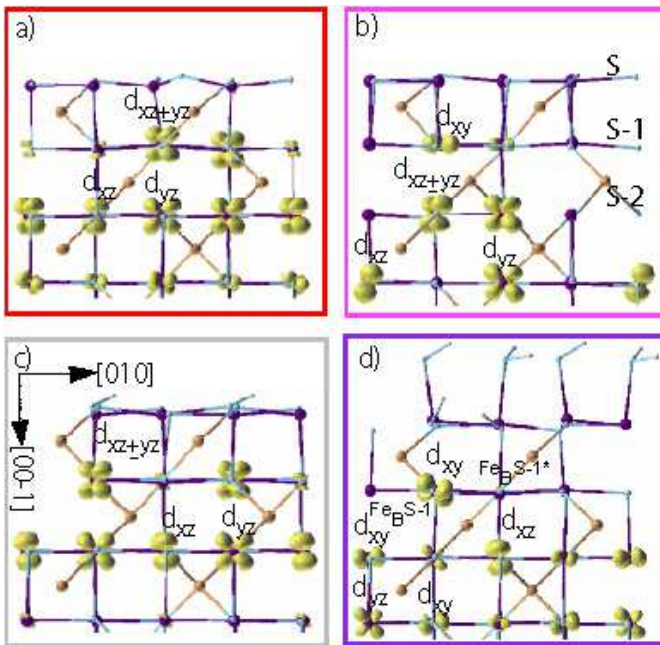


FIG. 4: Side view of the electron density integrated between -1.3 eV and E_F showing the occupation of the minority t_{2g} orbitals at the Fe_B -sites. a) B+V_O; b) B-layer; c) B+V_O+1H₂O(D); d) B+4H₂O(M). For the colour code see Fig. 1.

mination reaching several layers below the surface. Moreover, most of them violate the Anderson criterion: Fe_4O_4

cubes in the surface and subsurface layer are predominantly electron poor ($3Fe^{3+}+1Fe^{2+}$), while those in S-1 and S-2-layer are electron rich ($1Fe^{3+}+3Fe^{2+}$). Evidence for orbital ordering in thin magnetite films was reported recently from resonant soft x-ray diffraction [8].

The charge ordered state in the B-layer leads to the opening of a band gap of 0.3 eV as shown in Fig. 2d, consistent with previous calculations [18] and scanning tunneling spectroscopy measurements [40]. However the adsorption of water on the surface and the formation of surface hydroxyl groups leads to half-metallic behavior.

We have shown that on $Fe_3O_4(001)$ water tends to dissociate in oxygen vacancies or partially dissociate on the nondefective surface in contrast to the full dissociation found on $Fe_3O_4(111)$ [21, 41]. This adsorption mode is triggered by the presence of both Lewis acid and base sites on the surface and the intermolecular interaction as reported also on rutile(110) [42], anatase(001) [43] and $MgO(001)$ -surfaces [44]. The hydrogen bonded OH and H₂O can easily rearrange and thus provide adsorption sites for further species (e.g. heavy metal complexes). Our results indicate a pathway to manipulate e.g. the catalytic properties of transition metal oxide surfaces by triggering electron transfer processes and inducing new charge and orbitally ordered states via adsorbates.

We acknowledge discussions with G.E. Brown and T. Kendelewicz and support by the German Science Foundation (PE883/1-2) and a grant for computational time at the Leibniz Rechenzentrum Garching.

-
- [1] Z. Zhang and S. Satpathy, Phys. Rev. B **44**, 13319 (1991).
 [2] E.J.H. Verwey, Nature **144**, 327(1939).
 [3] J.H. Park *et al.*, Phys. Rev. B **55**, 12813 (1997).
 [4] D. Schrupp *et al.*, Europhys. Lett. **70**, 789 (2005).
 [5] J.P. Wright, J.P. Attfield, and P.G. Radaelli, Phys. Rev. Lett. **87**, 266401 (2001).
 [6] I. Leonov *et al.*, Phys. Rev. Lett. **93**, 146404 (2004).
 [7] H.-T. Jeng, G.Y. Guo, and D. J. Huang, Phys. Rev. Lett. **93**, 156403 (2004).
 [8] J. Schlappa *et al.*, Phys. Rev. Lett. **100**, 026406 (2008).
 [9] K. Ohe *et al.*, J. Chem. Eng. Jpn. **38**, 671 (2005).
 [10] H. Katsumata *et al.*, J. Environ. Manage. **69**, 187 (2003).
 [11] C. Martos *et al.*, Int. J. Hydrogen Energy **34**, 4475 (2009).
 [12] M.A. Henderson, Surf. Sci. Rep. **46**, 1 (2002).
 [13] P.A. Thiel and T.E. Madey, Surf. Sci. Rep. **7**, 211 (1987).
 [14] P. W. Tasker, J. Phys. C **12**, 4977 (1979).
 [15] S.A. Chambers, S. Thevuthasan, and S.A. Joyce, Surf. Sci. **450**, L273 (2000).
 [16] B. Stanka *et al.*, Surf. Sci. **448**, 49 (2000).
 [17] R. Pentcheva *et al.*, Phys. Rev. Lett. **94**, 126101 (2005).
 [18] Z. Lodziana, Phys. Rev. Lett. **99**, 206402 (2007).
 [19] R. Pentcheva *et al.*, Surf. Sci. **602**, 1299 (2008).
 [20] M. Fonin *et al.*, Phys. Rev. B **72**, 104436 (2005).
 [21] T. Kendelewicz *et al.*, Surf. Sci. **453**, 32 (2000).
 [22] C.H.F. Peden *et al.*, Catal. Today **51**, 513 (1999).
 [23] J.R. Rustad, A.R. Felmy, and E.J. Bylaska, Geochim. Cosmochim. Acta **67**, 1001 (2003).
 [24] T.K. Kundu *et al.*, J. Colloid Interface Sci. **295**, 364 (2006).
 [25] P. Blaha *et al.*, WIEN2k, An Augmented Plane Wave + Local Orbitals Program for Calculating Crystal Properties, (Karlheinz Schwarz, Techn. Univ. Wien, Austria), 2001. ISBN 3-9501031-1-2
 [26] J.P. Perdew *et al.*, Phys. Rev. Lett. **77**, 3865 (1996).
 [27] B. Santra, *et al.*, J. Chem. Phys. **127**, 184104 (2007).
 [28] B. Santra, *et al.*, J. Chem. Phys. **129**, 194111 (2008).
 [29] V.I. Anisimov *et al.*, Phys. Rev. B **48**, 16929 (1993).
 [30] We have varied U between 0-8 eV: Charge disproportionation at the Fe_B -sites is found beyond $U = 2$ eV.
 [31] H.P. Pinto and S.D. Elliot, J. Phys.: Condens. Matter **18**, 10427 (2006).
 [32] We have used muffin tin (MT) radii of $R_H^{MT} = 0.60$ Bohr, $R_{Fe}^{MT} = 1.90$, and $R_O^{MT} = 1.10$ and an energy cutoff for the wave functions and potential of $E_{max}^{wf} = 25$ Ry and $E_{max}^{pot} = 196$ Ry, respectively. For the integration in the Brillouin zone 16 $k||$ -points were used.
 [33] K. Reuter and M. Scheffler, Phys. Rev. B **65**, 035406 (2001); C.M. Weinert and M. Scheffler, Mat. Sci. Forum **10-12**, 25 (1986); M. Scheffler and J. Dabrowski, Phil. Mag. A **58**, 107 (1988).
 [34] A clean or water adsorbed half-occupied A-layer was

- found to be less stable in the pressure ranges studied here.
- [35] H. Over *et al.*, Phys. Rev. B **46**, 15438 (1992).
- [36] J. Rundgren, Phys. Rev. B **68** (2003) 125405.
- [37] N. Mulakaluri *et al.*, to be published.
- [38] For a filament current of 50 -100 nA a rough estimate of the electron dose is 1-2 (e/u. c.) per 10 s.
- [39] Only for B+V_O a configuration with Fe²⁺ in the surface layer competes with the configuration in Fig. 4a.
- [40] K. Jordan *et al.*, Phys. Rev. B **74**, 085416 (2006).
- [41] M.E. Grillo, M. W. Finnis, and W. Ranke, Phys. Rev. B **77**, 075407 (2008).
- [42] P. J. D. Lindan, N. M. Harrison, and M. J. Gillan, Phys. Rev. Lett. **80**, 762 (1998).
- [43] A. Vittadini *et al.*, Phys. Rev. Lett. **81**, 2954 (1998).
- [44] L. Giordano, J. Goniakowski, and J. Suzanne, Phys. Rev. Lett. **81**, 1271 (1998); M. Odelius, Phys. Rev. Lett. **82**, 3919 (1999).